

**Temporal variability
and spatial
distribution of IO**

R. Commane et al.

**Iodine monoxide at a clean marine coastal
site: observations of high frequency
variations and inhomogeneous
distributions**

**R. Commane^{1,*}, K. Seitz², C. S. E. Bale¹, W. J. Bloss³, J. Buxmann², T. Ingham^{1,4},
U. Platt², D. Pöhler², and D. E. Heard^{1,4}**

¹School of Chemistry, University of Leeds, LS2 9JT, UK

²Institute of Environmental Physics, University of Heidelberg, Germany

³School of Geography, Earth and Environmental Sciences, University of Birmingham, B15 2TT, UK

⁴National Centre for Atmospheric Science, University of Leeds, Leeds, LS2 9JT, UK
* now at: School of Engineering and Applied Sciences, Harvard University, MA, USA

Received: 24 January 2011 – Accepted: 27 January 2011 – Published: 8 February 2011

Correspondence to: D. E. Heard (d.e.heard@leeds.ac.uk)

Published by Copernicus Publications on behalf of the European Geosciences Union.

Title Page

Abstract

Introduction

Conclusions

References

Tables

Figures

◀

▶

◀

▶

Back

Close

Full Screen / Esc

Printer-friendly Version

Interactive Discussion



Abstract

The first in situ point observations of iodine monoxide (IO) at a clean marine site were made using a laser-induced fluorescence instrument deployed at Mace Head, Ireland in August 2007. IO mixing ratios of up to 49.8 pptv (1 s) were observed at day-time low tide, well in excess of previous observed spatially-averaged maxima. A strong anti-correlation of IO with tide height was evident and the high time resolution of the observations showed IO peaked in the hour after low tide. The temporal delay in IO peak compared to low tide has not been observed previously but coincides with the time of peak aerosol number previously observed at Mace Head.

A long path-differential optical absorption spectroscopy instrument (with a 2 × 6.8 km folded path across Roundstone Bay) was also based at the site for 3 days during the point measurement observation period. Both instruments show similar temporal trends but the point measurements of IO are a factor of ~6–10 times greater than the spatially averaged IO mixing ratios, providing empirical evidence of the presence of inhomogeneities in the IO mixing ratio near the intertidal region.

1 Introduction

The important role of iodine chemistry in the marine boundary layer has been highlighted by a number of studies (e.g., Alicke et al., 1999; O'Dowd et al., 2002). The iodine monoxide (IO) radical is involved in the catalytic destruction of ozone in the marine boundary layer (Davis et al., 1996). This destruction can be initiated by the reaction of IO with itself or BrO as well as with the HO₂ radical or NO₂. The reaction of IO with HO₂ alters the OH/HO₂ ratio (Bloss et al., 2005) and affects the oxidising capacity of the atmosphere, both directly (through HO_x) or indirectly through impacts on O₃ and NO_x. Iodine has been found in ultrafine particles (Mäkelä et al., 2002) and observations in the MBL have shown peaks in gas phase I₂ concentrations coincide with new particle bursts (O'Dowd et al., 2002; Sellegri et al., 2005). The self-reaction of

ACPD

11, 4533–4568, 2011

Temporal variability and spatial distribution of IO

R. Commane et al.

Title Page

Abstract

Introduction

Conclusions

References

Tables

Figures

◀

▶

◀

▶

Back

Close

Full Screen / Esc

Printer-friendly Version

Interactive Discussion



IO is also thought to lead to the formation and growth of these new particles, through the formation of higher iodine oxides (McFiggans et al., 2004; Kaltsayannis and Plane, 2008). If these new particles grow to form cloud condensation nuclei (CCN), they can influence cloud properties and have an impact on climate (Rosenfeld et al., 2008). Laboratory and modelling studies by Burkholder et al. (2004) suggested point mixing ratios of IO between 50 and 100 pptv were required to explain the particle bursts observed in coastal areas (O'Dowd et al., 2002).

IO radicals are formed through the reaction of atomic iodine with ozone. A steady state between IO and I atoms is formed during the day, with the reformation of ozone in the absence of other reactions:



In coastal areas, iodine atoms can be formed by the photolysis of molecular iodine or iodocarbons, which have been emitted from macroalgae in the intertidal zone and high concentrations of iodine atoms have been directly measured at a coastal site (Bale et al., 2008). IO was first observed at the site Mace Head Atmospheric Research Station (MH), located on the west coast of Ireland, in 1997 by Long Path Differential Optical Absorption Spectroscopy (LP-DOAS) (Alicke et al., 1999) and has since been measured a number of times, with varying concentrations of IO observed, up to a maximum of 7 pptv (Saiz-Lopez et al., 2006a). These previous spatially-averaged observations of IO at MHARS have provided important information about the role of macroalgae in initiating iodine chemistry through the emission of molecular iodine (e.g., McFiggans et al., 2004) and, to a lesser extent, iodocarbons (e.g., Carpenter et al., 2001). These studies also linked iodine species to new particle formation (O'Dowd et al., 2002) and initiated chamber studies into the role of specific macroalgae in the emission of iodine (Bale et al., 2008; Dixneuf et al., 2009; Ball et al., 2010).

Most field observations of IO have been made by LP-DOAS instruments, which use path lengths of several kilometres to improve the LP-DOAS sensitivity. This significant

Temporal variability and spatial distribution of IO

R. Commane et al.

Title Page

Abstract

Introduction

Conclusions

References

Tables

Figures

◀

▶

◀

▶

Back

Close

Full Screen / Esc

Printer-friendly Version

Interactive Discussion



Temporal variability and spatial distribution of IO

R. Commane et al.

Title Page

Abstract

Introduction

Conclusions

References

Tables

Figures

◀

▶

◀

▶

Back

Close

Full Screen / Esc

Printer-friendly Version

Interactive Discussion



spatial averaging can conceal the presence of an inhomogeneous distribution of the target species along the LP-DOAS light-path (Saiz-Lopez et al., 2006a), which can make the interpretation of point observations of short-lived species (e.g. OH and HO₂) difficult. A factor of 10 increase in the IO concentration observed by LP-DOAS was required to reproduce [HO_x] observed during the North Atlantic Marine Boundary Layer Experiment (NAMBLEX) campaign (Sommariva et al., 2006). A recent LP-DOAS study with various path lengths found similar IO column densities for both a 2 km and 10 km path length above beds of macroalgae, indicating the presence of significant inhomogeneities within the light path (Seitz et al., 2010).

We present point observations of IO made using a portable and compact Laser-Induced Fluorescence (LIF) instrument developed for the detection of IO. The instrument and calibration method are described. The temporal and tidal related variations of the in situ point observations of IO are discussed and the short-term variability investigated. The point observations of IO are compared to the spatially-averaged IO observations made by the LP-DOAS instrument and the extent of the inhomogeneity of the IO concentrations is examined.

2 Instrumentation

2.1 Site description

The Mace Head Atmospheric Research Station (MH) (53.32° N, 9.90° W) is a clean marine site located on the west coast of Ireland (Fig. 1). The research station has been the subject of extensive halogen studies in the past (e.g., Alicke et al., 1999; Saiz-Lopez et al., 2006a) and is described extensively in Heard et al. (2006).

Mace Head experiences semi-diurnal tides, with extensive beds of macroalgae exposed in narrow strips along the coast at low tides. A log of the approximate low and high tide times at the site was maintained during August 2007 and the high and low tide times were found to agree well with the tide times predicted for Roundstone Bay (7 km

**Temporal variability
and spatial
distribution of IO**

R. Commane et al.

Title Page

Abstract

Introduction

Conclusions

References

Tables

Figures

◀

▶

◀

▶

Back

Close

Full Screen / Esc

Printer-friendly Version

Interactive Discussion



north) by the UK Hydrographic Office (UKHO) Poltis program. During the measurement period, the intertidal height in Roundstone Bay varied between 1 m at Neap Tide and 4.5 m at Spring Tide, which corresponds to a horizontal distance of between ~ 50 m (high tide) and ~ 100 m (low tide) in front of the site. During the observation period, the wind direction varied from west to north-west, with wind speeds varying from 11 m s^{-1} to 0.5 m s^{-1} (data courtesy of B. Kelly, Met Éireann). 24 h back trajectory calculations show this air had travelled at low level over the ocean for most of the previous 24 h.

Point measurements of IO were made on eight days between 15 and 30 August 2007 with short breaks in data collection due to restrictions on the deployment of the sampling cell i.e. observations were only possible when the station was attended and were not possible during inclement weather conditions. The instrument was installed in a van located ~ 5 m north of the site buildings. The portable fluorescence cell was extended 10 m away from the van, towards the sea (upwind), giving it ~ 5 m clearance in front of the site buildings, approximately 100 m from the low tide line and exposed macroalgae. Simultaneous spatially-averaged measurements were made by the LP-DOAS instrument for the final three LIF observation days (28–30 August 2007). The LP-DOAS instrument was located in the site buildings with the light-path passing 5 m behind the LIF fluorescence cell to a retro-reflector located across Roundstone Bay (total path length 13.6 km).

2.2 Laser-induced fluorescence instrument

The laser-induced fluorescence (LIF) instrument uses radiation at $\lambda = 444.885 \text{ nm}$ (generated by a tunable solid state laser) to excite the (2,0) band of the $A^2\Pi_{3/2} \leftarrow X^2\Pi_{3/2}$ electronic transition (R1 bandhead), which consists of several overlapping rotational lines (Gravestock et al., 2010). Off-resonance fluorescence in the (2,5) band is detected at $\lambda = 520.3 \text{ nm}$.

The instrument is a more compact version of an instrument described in Whalley et al. (2007) and Furneaux et al. (2010) and was constructed around the Leeds aircraft

instrument for OH and HO₂ measurements (Commane et al., 2010). Details of the laser excitation and fluorescence spectra, and the photophysical and collisional processes occurring in the $A^2\Pi_{3/2}$ state of IO can be found in Gravestock et al. (2010). Installed on two aircraft racks, with a separate pump set, calibration system and portable fluorescence cell, the instrument was characterised prior to, and calibrated during, deployment at Mace Head.

The optical cell is similar in design to that described in Commane et al. (2010), with an extended inlet to reduce solar scattered light. The inlet was pointed vertically upwards and consisted of a 45 mm internal diameter stainless steel cylinder, with a 25 mm internal diameter solid nylon cylinder of 21.5 cm length inserted between a stainless steel cap and base, giving a total length of 33 cm. A maximum of $\approx 5 \text{ cts s}^{-1}$ of solar scattered light was observed within the cell at solar noon. A 0.8 mm pinhole was centered on a flat disc, drawing ambient air into the fluorescence cell at a flow rate of 8.5 slm, giving an cell pressure of ~ 150 Torr.

A Nd:YAG laser (9.1–9.5 W of $\lambda = 532$ nm radiation) was used to pump a Ti:sapphire laser cavity, generating up to 1.1 W of $\lambda \approx 890$ nm radiation (~ 35 ns pulse width (FWHM), 0.065 cm^{-1} laser linewidth). The incident angle of the intra-cavity diffraction grating was tilted using a stepper motor to vary the wavelength. The $\lambda \approx 890$ nm light was passed through a cerium lithium borate (CLBO) doubling crystal producing up to 100 mW of blue light at $\lambda \approx 445$ nm. The beam was split using dielectric coated beam splitting plates on a fibre launcher contained within the laser casing and 96% of the $\lambda \approx 445$ nm light was delivered to the fibre with $\sim 75\%$ transmitted to the IO fluorescence cell through the 15 m fibre optic cable. The remaining $\lambda \approx 445$ nm light (4%) was delivered to a photodiode shielded from ambient light, which was calibrated to the laser power exiting the cell, allowing continuous measurement of laser power. A wavemeter (Coherent Wavemaster, resolution ± 0.001 nm, accuracy ± 0.005 nm) was used to determine the wavelength of detected light.

Laser radiation was delivered to the cell through a 15 m fibre optic cable (Oz Optics) and the light exiting the fibre was collimated and focussed through a baffled side-arm

Temporal variability and spatial distribution of IO

R. Commane et al.

Title Page

Abstract

Introduction

Conclusions

References

Tables

Figures

◀

▶

◀

▶

Back

Close

Full Screen / Esc

Printer-friendly Version

Interactive Discussion



Temporal variability and spatial distribution of IO

R. Commane et al.

Title Page

Abstract

Introduction

Conclusions

References

Tables

Figures

⏪

⏩

◀

▶

Back

Close

Full Screen / Esc

Printer-friendly Version

Interactive Discussion



into the fluorescence region. Fluorescence was detected on an axis perpendicular to both the laser beam and ambient airflow, and passed through a 50.2 mm diameter window (with $\lambda = 521$ nm anti-reflection coating), was collimated and filtered by a $\lambda = 521$ nm centred interference filter (Barr Associates, 2 nm FWHM, 52% transmission) and focussed through two lenses (50.2 mm diameter, 52 mm focal length, anti-reflection coated for $\lambda = 521$ nm) onto the photocathode of a yellow sensitive channel photomultiplier (CPM) (Perkin Elmer, C993 P). The signal from the CPM was sent to a photon-counting card (Becker and Hickl, MSA 300) in the data-acquisition computer before the signal was processed. The photon-counting card was triggered by a timed-transistor logic (TTL) pulse from the delay generator 50 ns prior to the laser pulse.

Photons at $\lambda = 521$ nm from the laser focal volume were recorded during two time gates: i) Gate *A*: a 100 ns wide collection gate centred directly over the laser pulse to collect the LIF signal, laser scattered (~ 0.8 – 1 cts s^{-1} mW^{-1}) and solar scattered light (maximum ~ 5 cts s^{-1}) and ii) Gate *B*: a 1000 ns wide collection gate, delayed 50 μ s after the laser pulse to collect the signal due to solar scattered light and CPM dark counts (the latter ~ 0.01 cts s^{-1}). The difference in signal (cts s^{-1}) between gates *A* and *B* is recorded as the 1 s averaged IO fluorescence signal and can be integrated to longer time periods as required. During all field measurements, a 1:1 duty cycle was adopted: the laser wavelength was tuned to the *online* wavelength (444.887 nm) for 60 s, producing a one minute online point (or 300 000 laser shots), then tuned offline (444.882 nm) for 60 s, producing 60 one second offline points. From these 1 s data, the data were usually averaged to generate a 1 min data point. The signals are normalised for laser power and the mean offline signal is subtracted from the mean online signal to give the laser normalised signal (Sig_{IO} , cts s^{-1} mW^{-1}). Finally, this signal is divided by the sensitivity to give the IO concentration ($[IO]$, molecule cm^{-3}):

$$[IO] = \frac{Sig_{IO}}{C_{IO}} \quad (1)$$

where C_{IO} is the instrument sensitivity to IO ($\text{cts s}^{-1} \text{mW}^{-1} \text{molecule}^{-1} \text{cm}^3$). Using the ambient temperature and pressure recorded during the IO measurement period, the IO mixing ratio was then calculated.

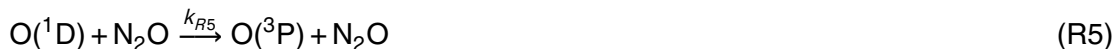
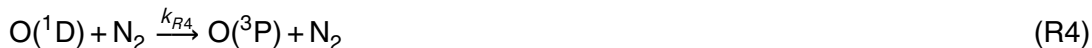
2.2.1 IO calibration

Laser-induced fluorescence spectroscopy is not an absolute technique and the sensitivity of the instrument to IO must be determined by calibration. A turbulent-flow calibration system was developed to produce known concentrations of IO. The sensitivity of the instrument did not found to vary throughout the measurement period and a sensitivity of $0.039(\pm 0.001) \text{cts s}^{-1} \text{mW}^{-1} \text{pptv}^{-1}$ was used for all data analysis.

A variable flow of N_2O (BOC, 98% N_2O in N_2 -medical grade; ~ 375 sccm) was mixed with excess CF_3I (Aldrich, 99%) in a 50 slm (standard litres per minute) flow of nitrogen (BOC, OFN) at atmospheric pressure. The gas mixture was passed through a square aluminium tube ($1.27 \text{cm} \times 1.27 \text{cm} \times 30 \text{cm}$) and the N_2O in the turbulent flow was photolysed ($\lambda = 184.9 \text{nm}$) using a mercury lamp to produce a known concentration of $\text{O}(^1\text{D})$:



The photolysis product $\text{O}(^1\text{D})$ is rapidly quenched to $\text{O}(^3\text{P})$ by N_2O and N_2 as well as reacting with N_2O :



The fraction of $\text{O}(^1\text{D})$ quenched to $\text{O}(^3\text{P})$ (Ω) is calculated as:

$$\Omega = \frac{k_{R4} [\text{N}_2] + k_{R5} [\text{N}_2\text{O}]}{k_{R4} [\text{N}_2] + k_{R5} [\text{N}_2\text{O}] + k_{R6} [\text{N}_2\text{O}]} \quad (2)$$

Temporal variability and spatial distribution of IO

R. Commane et al.

Title Page

Abstract

Introduction

Conclusions

References

Tables

Figures

◀

▶

◀

▶

Back

Close

Full Screen / Esc

Printer-friendly Version

Interactive Discussion



Quenching to O(³P) occurs in less than 1.6 ns and under most conditions, over 98% of O(¹D) is quenched to O(³P), which reacts with CF₃I to produce IO:



With CF₃I in excess in Reaction R7 ensuring pseudo-first-order conditions, the rate of production of IO was determined by the rate of generation of O(³P). In the photolysis region, the concentration of IO is given by:

$$[\text{IO}] = [\text{N}_2\text{O}] \sigma_{\text{N}_2\text{O}} \phi_{\text{IO}} \Omega F_{184.9\text{nm}} \partial t \quad (3)$$

where $\sigma_{\text{N}_2\text{O}}$ is the absorption cross-section of N₂O at 184.9 nm ($\sigma_{\text{N}_2\text{O}} = 1.43 \times 10^{-19} \text{ cm}^2 \text{ molecule}^{-1}$, Sander et al., 2006), ϕ_{IO} is the chemical yield of IO from Reaction R7 ($\phi_{\text{IO}} = 0.83$, Gilles et al., 1996), $F_{184.9\text{nm}}$ is the photon flux of the lamp at $\lambda = 184.9 \text{ nm}$ and ∂t is the irradiation time. The product $F_{184.9\text{nm}} \partial t$ is determined by N₂O actinometry (Commane et al., 2010).

Figure 2 shows a calibration over a range of ambient concentrations from 2.2 pptv ($5.4 \times 10^7 \text{ molecule cm}^{-3}$) to 37.2 pptv ($9.2 \times 10^8 \text{ molecule cm}^{-3}$), which can be generated by varying both [N₂O] ($1.2\text{--}8 \times 10^{16} \text{ molecule cm}^{-3}$) and the lamp flux at $\lambda = 189 \text{ nm}$ ($9.5 \times 10^{12}\text{--}2.5 \times 10^{13} \text{ photon cm}^{-2} \text{ s}^{-1}$).

The total uncertainty in the IO calibration was found to be 23.5% at 1 σ . This is the sum in quadrature of the uncertainty in the laser power (1%), the lamp flux (11%), the absorption cross-section of N₂O (<1%), the chemical yield of IO from Reaction R7 (11%), the concentration of N₂O (1%) and the reproducibility of the wavemeter to accurately find the excitation wavelength of IO (18%), which was determined from experimental tests with a constant calibration source.

The limit of detection (LOD) of the instrument is determined by both the sensitivity to IO (C_{IO}) and the instrumental noise. For equal online and offline sample sizes with equal variance, the minimum detectable IO signal, $\text{IOSig}_{\text{min}}$, for a given confidence interval (CI) can be calculated:

Temporal variability and spatial distribution of IO

R. Commane et al.

[Title Page](#)[Abstract](#)[Introduction](#)[Conclusions](#)[References](#)[Tables](#)[Figures](#)[◀](#)[▶](#)[◀](#)[▶](#)[Back](#)[Close](#)[Full Screen / Esc](#)[Printer-friendly Version](#)[Interactive Discussion](#)

$$\text{IOSig}_{\min} = T_{\text{Cl}} \sqrt{\frac{2}{m}} \sigma_{\text{IO}} \quad (4)$$

where T_{Cl} is the T value for a given confidence interval ($T_{95\%} = 2$), m is the sample size defined by the sampling frequency and σ_{IO} is the standard deviation of the background, which is assumed to be representative of the standard deviation of the online sample.

Assuming the background signal obeys Poisson Statistics (Whalley et al., 2007), the standard deviation of the total background signal is defined as the square root of the mean:

$$\sigma_{\text{IO}} = \sqrt{(S_{\text{lb}} + S_{\text{sb}} + S_{\text{dc}})} \quad (5)$$

where S_{lb} is the signal due to laser scatter, S_{sb} is the signal due to solar background and S_{dc} are the dark counts of the CPM and $S_{\text{lb}} + S_{\text{sb}} + S_{\text{dc}}$ is the mean of the sum of these (S_{BG}). For a 60 s measurement cycle at noon on 29 August, the limit of detection was calculated to be 1.25 pptv (composed of $T_{95\%} = 2$, $P_{\text{IO}} = 44.8$ mW, $C_{\text{IO}} = 0.039$ cts s^{-1} mW^{-1} pptv $^{-1}$, $S_{\text{BG}} = 35.7$ cts s^{-1} , Solar Signal = 1.8 cts s^{-1} , $m = 60$).

IOSig_{\min} is converted into a minimum detectable mixing ratio of IO (pptv) by:

$$\text{IO}_{\min} = \frac{\text{IOSig}_{\min}}{C_{\text{IO}} P_{\text{IO}}} \quad (6)$$

where C_{IO} is the instrument sensitivity to IO (cts s^{-1} mW^{-1} pptv $^{-1}$) and P_{IO} is the laser power in the IO cell (mW).

2.2.2 Influence of NO₂

NO₂ exhibits a pressure-broadened absorption spectrum in the wavelength range used for IO excitation ($\lambda = 444\text{--}445$ nm) and fluorescence from NO₂ excited in this region includes the wavelength region transmitted through the band-pass interference filter ($\lambda = 521$ nm). Tests were conducted on the instrument to determine the effect of NO₂.

Temporal variability and spatial distribution of IO

R. Commane et al.

Title Page

Abstract

Introduction

Conclusions

References

Tables

Figures

◀

▶

◀

▶

Back

Close

Full Screen / Esc

Printer-friendly Version

Interactive Discussion



It was found that no response in signal above the calculated instrumental LOD was observed for NO₂ mixing ratios below 500 ppbv, which is far less than the sub-ppbv levels of NO₂ observed at clean marine sites. With the addition of over 500 ppbv NO₂, the instrument recorded a response of -0.004 pptv of false IO per ppbv of NO₂, again much less than the instrument uncertainty. Thus, any interference from constant background NO₂ mixing ratios would result in only a small underestimate of IO recorded.

3 Point observations of IO

Point observations of IO were made over eight days in August 2007 and encompassed diel cycles of high and low tides. Figure 3 shows the observed time series of the IO mixing ratio (pptv) for 60 s time integration, where the IO mixing ratio showed a strong dependence on tide height. The highest IO mixing ratio of 29.3 pptv (60 s integration time) was observed at low spring tide around noon on 29 August (spring tide; tidal height range of 4.5 m over 24 h). At the neap tide (tidal height range of 1 m in 24 h), a maximum IO mixing ratio of 4 pptv was observed. The lowest neap tides occurred at dawn and dusk so the photolysis rate of photolabile sources of I atoms will be significantly lower than at mid-day and result in reduced I atom production. It is possible, and indeed probable, that neap tides at mid-day would result in greater IO mixing ratios than observed here.

3.1 Temporal variability of IO

Figure 4(a) shows a short section of IO data (over 2 min) recorded at 1 s resolution close to low tide with both online and background signal (also recorded at 1 s resolution). Up to 49.7 (± 8.6) pptv of IO was observed over a 1 s integration time at the lowest tide on 29 August, the highest mixing ratio of IO observed at Mace Head to date. Within this 60 s measurement period, the online IO mixing ratio (red) varies between 10.0 pptv and 49.7 pptv. The variation in the offline signal (cts s⁻¹; black) illustrates the

Temporal variability and spatial distribution of IO

R. Commane et al.

Title Page

Abstract

Introduction

Conclusions

References

Tables

Figures

◀

▶

◀

▶

Back

Close

Full Screen / Esc

Printer-friendly Version

Interactive Discussion



range of instrumental variation expected (converted to an equivalent IO mixing ratio), which is much less than that observed in ambient observations. The offline signal is below the 1 s (2σ) instrumental limit of detection (blue line).

IO mixing ratios of up to 50 pptv are significantly greater than any spatially-averaged IO mixing ratio reported to date and provide further evidence of the role of IO in new particle formation. Modeling studies suggested that IO mixing ratios of the order of 50 pptv would be required to explain new particle formation initiated by the IO self reaction (Burkholder et al., 2004):



Kaltsayannis and Plane (2008) suggest the growth of particles proceeds through higher oxide formation and Furneaux et al. (2010) found that point observations of IO by LIF were correlated with sub-10 nm particle number (up to 15 pptv IO and $18 \times 10^4 \text{ cm}^{-3}$ particle number).

Figure 4b shows the 60 s data around spring tide with the standard deviation of the 1 s data within this mean shown as a \pm error bar. The variability of the 1 s IO data at daytime low tide is much greater than during the night or high tide and suggests that the nearby macroalgae (a source of halocarbons and molecular iodine) are not steadily emitting IO precursor species, perhaps as a result of wave action or changing wind speeds.

3.2 Diel and tidal dependance of IO

The tidal variation of IO shows two distinct modes associated with the diel cycle (Fig. 5). During the day, a clear anti-correlation of IO with tide height can be seen and the highest IO mixing ratios were observed around daytime low tide. These daytime data were highly variable on all days with IO mixing ratios between 3 and 29 pptv (60 s integration time) observed at low tide.

Temporal variability and spatial distribution of IO

R. Commane et al.

Title Page

Abstract

Introduction

Conclusions

References

Tables

Figures

◀

▶

◀

▶

Back

Close

Full Screen / Esc

Printer-friendly Version

Interactive Discussion



Temporal variability and spatial distribution of IO

R. Commane et al.

Title Page

Abstract

Introduction

Conclusions

References

Tables

Figures

◀

▶

◀

▶

Back

Close

Full Screen / Esc

Printer-friendly Version

Interactive Discussion



Seaweed surveys at Mace Head over various tide heights found that macroalgae are widely distributed in narrow tidal strips a few metres wide directly in front (and upwind) of the research station. A visual inspection of the area in front of the LIF observation point showed no macroalgae were exposed at tide heights greater than ~ 3 m (high tide). The observed IO mixing ratios were of a similar range during day and night for these high tides heights. This suggest that any open ocean iodine sources were not sufficient to allow detection of IO at the LIF sampling point. At tide heights between 3 and 1 m macroalgae species such as *Palmaria palmata*, *Ascophyllum nodosum* and various type of *Fucus* were present and a maximum IO mixing ratio of 8.2 pptv was observed during the day. At low tides below 1 m, large beds of *Laminaria digitata* were exposed directly in front of the LIF sampling point and mixing ratios of IO up to 29.3 pptv were observed.

3.2.1 Temporal offset from low tide

Defining a common time basis based on hours from low tide (Tidal Time) allows the continuous 60 s IO data series on the final three days of measurements (as shown in Fig. 4b) to be considered together. Figure 6 shows the 60 s IO data on this common time basis. Overall the time of the IO enhancement (IO greater than the limit of detection) averages to about five hours around daytime low tide. Although the maximum observed IO occurred before low tide (29 August), overall the mean IO detected in the hour after low tide (13.7 pptv) is greater than before low tide (8.4 pptv) and most of the IO above 12 pptv (*peak* IO) is concentrated in the hour after low tide.

The time delay between low tide and peak IO coincides with the sharp increase in sub-10 nm particle number observed in the hour after low tide during the PARFORCE and BIOFLUX campaigns at Mace Head (O'Dowd and Hoffmann, 2005), suggesting IO plays a key role in new particle formation. Unfortunately, aerosol measurements were not made at Mace Head during the observation period of this study precluding direct correlation with the IO data. At Mweenish Bay, 6 km south of Mace Head Seitz et al. (2010) found that nucleation events coincided with peak IO, while, at a polluted site

in Roscoff, France, Furneaux et al. (2010) found that ultra fine particles were generally observed around the same time as the highest IO mixing ratios, with the IO mixing ratio showed a temporally broader peak. However with multiple locations of macroalgae and variable wind directions, determining the exact relationship between IO and new particles was difficult during the Roscoff study.

At mid-latitude coastal marine boundary layer sites, molecular iodine emission from macroalgae in the intertidal zone has previously been identified as a major source of IO (McFiggans et al., 2004). Küpper et al. (2008) propose that the ozone-scavenging reactivity of iodide on kelp surfaces at low tide leads to the direct release of molecular iodine from *Laminaria* into the coastal atmosphere. The emission of iodine from *Laminaria* has also been linked to dessication and physical agitation (Bale et al., 2008; Ball et al., 2010). Therefore, the time delay between low tide and the peak IO observed here could be attributed to the time required for the *Laminaria* to dry out and emit I₂. The physical agitation caused by wave motion as the tide returns could contribute to the large variability seen in the 1 s IO data. Although recent chamber studies have suggested iodine emission from *Laminaria* may also occur in cycles independently of physical agitation (Dixneuf et al., 2009).

At times of highest IO, macroalgae were located a maximum of ~ 100 m upwind of the LIF sampling point and, with mean wind speeds of ~ 5 m s⁻¹ at this time, the mean chemical processing time between emission and sampling was ~ 20 s. This suggests that I₂ (with a photolysis lifetime of 10 s at mid-day) is the dominant source of I atoms and the major precursor to IO at Mace Head. However, with a prevailing westerly wind and wind speeds of 5–10 m s⁻¹ typical in the area, it is possible that the maximum IO mixing ratio, greatest O₃ destruction and peak in particle formation all occur inland from the observation point at Mace Head.

Temporal variability and spatial distribution of IO

R. Commane et al.

Title Page

Abstract

Introduction

Conclusions

References

Tables

Figures

◀

▶

◀

▶

Back

Close

Full Screen / Esc

Printer-friendly Version

Interactive Discussion



3.2.2 Night-time IO

At night, there is no tidal dependence evident in the IO mixing ratios. Figure 7 shows the probability distribution of the IO mixing ratio observed at night. The observations are distributed around zero, within the mean instrumental limit of detection (2σ), with a slight negative bias (-0.49 pptv). Previous observations of IO at night at Mace Head were associated with high NO_3 mixing ratios and the only known IO production pathway at night is through the reaction of I_2 with NO_3 :



where $k_{R10} = 1.5 \times 10^{-12} \text{ cm}^3 \text{ molecule}^{-1} \text{ s}^{-1}$, (Chambers et al., 1992) and $k_{R11} = 1.2 \times 10^{-12} \text{ cm}^3 \text{ molecule}^{-1} \text{ s}^{-1}$ at 298 K (Sander et al., 2006).

During the LIF measurement period, mixing ratios of NO_3 were found to be below the LP-DOAS limit of detection of 4.8 pptv, while a maximum I_2 mixing ratio of 65 pptv was observed at night by LP-DOAS. Saiz-Lopez et al. (2006b) showed that the spatially-averaged I_2 observed by LP-DOAS was concentrated in a short distance over the intertidal area and mixing ratios of greater than 65 pptv are probable and up to 100 pptv I_2 is possible Bitter et al. (2005). Given typical ozone mixing ratios of ~ 30 ppbv, an upper limit of 4.8 pptv of NO_3 and an estimated 200 ppt of I_2 , the IO formation rate is about 0.03 pptv s^{-1} . This requires a minimum of 40 s to form sufficient IO for detection by the LIF instrument (2σ LIF limit of detection = 1.46 pptv). With windspeeds of $5\text{--}10 \text{ m s}^{-1}$ at the site, the transit time of air passing between the macroalgae exposed at low tide to the LIF sampling point is between 10 and 20 s, which is insufficient time for detectable mixing ratios of IO to be formed.

Temporal variability and spatial distribution of IO

R. Commane et al.

[Title Page](#)[Abstract](#)[Introduction](#)[Conclusions](#)[References](#)[Tables](#)[Figures](#)[⏪](#)[⏩](#)[◀](#)[▶](#)[Back](#)[Close](#)[Full Screen / Esc](#)[Printer-friendly Version](#)[Interactive Discussion](#)

4 Comparison of spatially-averaged and point observations of IO

For three days around low tide at Mace Head, IO was measured by a long-path Differential Optical Absorption Spectroscopy (LP-DOAS) instrument from the University of Heidelberg (Huang et al., 2010). The wind was consistently arriving at the site from the west to north-west for all three days, allowing direct comparison of spatially-averaged and point measurements of IO.

4.1 Long path – DOAS instrument

Differential Optical Absorption Spectroscopy (DOAS) (Platt and Stutz, 2008) is a well established technique to identify and quantify trace gases by their narrow band absorption structures. The setup of the active long-path DOAS (LP-DOAS) systems used was a further development of the coaxial mirror system introduced by Axelson et al. (1990). A detailed description of the Fibre LP-DOAS can be found in Merten et al. (2009). The light path (6.8 km one-way) crossed Roundstone Bay to Roundstone about 10 m a.s.l. at high tide (Fig. 1), where a reflector consisting of 76 quartz prisms (63 mm diameter) was located. The reflected light was analyzed by a spectrometer (Acton Spectra Pro 300, $f = 4.1$, 1900 gr mm^{-1}). The detector used was a 1024 pixel photodiode array detector (type Hamamatsu S3904-1024). IO was measured in the 416–439 nm wavelength range, with a 10 min integration time. For the analysis the software DOASIS (Kraus, 2005) was used to simultaneously fit the different references to the atmospheric spectrum using a non-linear least-squares method (e.g., Stutz and Platt, 1996). In addition, a polynomial of 5th order was included to account for broad band structures due to scattering in the atmosphere. As well as the IO cross section (Spietz et al., 2005), references of NO_2 (Voigt et al., 2002), and H_2O (Rothman et al., 2005) were included in the fitting procedure. NO_3 was analysed between 618 and 626 nm and 657 and 664 nm and fitted using NO_3 (Yokelson et al., 1994) and H_2O vapour cross sections. Over the three days discussed here, NO_3 mixing ratios were not observed above the detection limit of 4.8 pptv.

Temporal variability and spatial distribution of IO

R. Commane et al.

Title Page

Abstract

Introduction

Conclusions

References

Tables

Figures

◀

▶

◀

▶

Back

Close

Full Screen / Esc

Printer-friendly Version

Interactive Discussion



4.2 Data comparison

Figure 8 shows the time series of both the LIF and LP-DOAS IO mixing ratios. The general trend of higher IO at daytime low tide is reproduced by both instruments but the LIF IO mixing ratios are much greater than the spatially averaged LP-DOAS IO mixing ratios. Over this 10 min integration time, the maximum IO measured by LP-DOAS was 4.4 pptv.

The ratio of IO point measurements to spatially averaged measurements indicates the extent of the spatial distribution throughout the DOAS light beam. This ratio was found to change over the three days of measurements as the tidal structure changed.

An increase in IO at low tides is present in the spatially averaged LP-DOAS observations but to much less of an extent than that seen in the point observations. Figure 8c shows the anti-correlation of the LIF/LP-DOAS ratio with tide height. On 28–29 August, the maximum ratio reaches 9.8. Back-trajectory analysis shows the air arriving at the site on these days was north-westerly. On 30 August, the ratio reaches a maximum of 5.5 and coincides with the highest IO observed by LP-DOAS. Back-trajectory analysis showed the wind was more westerly on 30 August, resulting in the air spending less time traveling over the macroalgae beds before being sampled by the LIF instrument. Below tide heights of ~ 0.3 m, additional *Laminaria* was also exposed at the retro-reflector end of the LP-DOAS light path, that had not been exposed on previous days. This increased inhomogeneity in IO sources may account for the sharp decrease in the LIF/LP-DOAS ratio observed below these tide heights on 30 August.

The point observations of IO presented in this study provide the first direct experimental evidence of the extent of the spatial inhomogeneity of IO along the DOAS light path at Mace Head. Evidence of inhomogeneities in IO have been observed at coastal sites previously. At Mweenish Bay (6 km south of Mace Head), Seitz et al. (2010) found inhomogeneities in IO mixing ratios from LP-DOAS light paths of various lengths positioned directly above beds of macroalgae. Comparison of spatially averaged I_2 observed by LP-DOAS and point measurements by CRDS have already highlighted the

Temporal variability and spatial distribution of IO

R. Commane et al.

Title Page

Abstract

Introduction

Conclusions

References

Tables

Figures

◀

▶

◀

▶

Back

Close

Full Screen / Esc

Printer-friendly Version

Interactive Discussion



inhomogeneity in the iodine distribution along the LP-DOAS light path at Mace Head (Saiz-Lopez et al., 2006b). Model calculations suggested that all the I_2 was located in a narrow coastal band of less than 10% of the total light-path. Due to a lack of point observations of IO at that time, it was not possible to prove this hypothesis for IO, but local IO mixing ratios of up to 47 pptv were suggested from the I_2 /IO ratio observed by LP-DOAS. This predicted inhomogeneity is in good agreement with the point observations of IO presented here. Another study at Roscoff, France found point observations of IO were only a factor of 2–3 higher than spatially averaged IO (Furneaux et al., 2010; Wada et al., 2007). This study will be discussed in detail in Sect. 4.3.1.

4.3 Implications of inhomogeneities in IO

The presence of high concentrations of iodine monoxide leads to a number of effects on the local chemistry, including oxidative capacity and the potential for new particle formation.

4.3.1 Evolution of IO with tide height

The daytime point observations of IO by LIF were found to be anti-correlated with tide and can be quantified as:

$$IO = 17.75e^{-TH/1.08} + 0.02, \quad (7)$$

where IO is in pptv and TH is tide height in metres. This is a stronger correlation with tide height than seen previously at Mace Head. The LP-DOAS light beam sampled over ocean for more than 90% of the light path so a weaker correlation of IO with tide height is expected. Figure 9 shows how a relationship of $IO = 3.07e^{-TH/1.29} + 0.44$ observed by the LP-DOAS during this study compares to a previous study by Carpenter et al. (2001), which found an exponential correlation of $IO = 2.6e^{-TH/1.7}$. The LP-DOAS path-length during Carpenter et al. (2001) was 14.6 km compared to the LP-DOAS path-length of 13.6 km used here, resulting in greater spatial averaging in the Carpenter

Temporal variability and spatial distribution of IO

R. Commane et al.

Title Page

Abstract

Introduction

Conclusions

References

Tables

Figures

⏪

⏩

◀

▶

Back

Close

Full Screen / Esc

Printer-friendly Version

Interactive Discussion



et al. (2001) study. Both paths were to Roundstone to the north of Mace Head. It is probable that the high mixing ratios of IO observed by the LIF instrument here were previously masked by both the long time (30 min) and spatial averaging (14 km) of LP-DOAS measurements.

At a polluted site in Roscoff, Northern France (mentioned above), Furneaux et al. (2010) found that point measurements of IO by LIF were only a factor of 2–3 greater than spatially averaged LP-DOAS measurements. The IO by LIF relationship with tide was determined to be $IO = 10.05e^{-TH/2.8} - 0.34$. This slightly weaker correlation than observed by LIF at Mace Head may be due to the more dispersed sources of IO and the titration of IO by the higher NO_x mixing ratios present at Roscoff. IO may also have been chemically consumed or lost to new particle formation during the long transit time between the widely dispersed macroalgae and the sampling point.

4.3.2 Impact on oxidation

During the day, O_3 can be photolysed to form $O(^1D)$ (leading to OH formation) and studies at a coastal site in France found that ozone deposition peaked during low tide (Whitehead et al., 2009). O_3 can also be destroyed by reaction with I atoms to form IO (Reaction R1). The combination of these processes may explain the 5 ppbv reduction in ozone observed around low tide on 30 August 2007 (Fig. 10).

It is unlikely that the macroalgae located within 10–20 s transport time of the sampling cell was the source of ozone-depleting iodine, as the reaction of O_3 with I atoms to produce IO is too slow for O_3 to be appreciably depleted within this time. McFiggans et al. (2004) calculated an O_3 depletion rate of 0.1 ppbv h^{-1} from the self-reaction of 5 pptv of IO. This, while significant, is too slow for the depletion to be observed so close to the iodine emission point. For the greater than 10 pptv of IO observed at the site at low tide (linked to the emission of iodine from macroalgae directly in front of the observation point), O_3 destruction is likely to take place significantly downwind and, given the wind direction, inland from the site. This suggests that the ozone depletion

Temporal variability and spatial distribution of IO

R. Commane et al.

Title Page

Abstract

Introduction

Conclusions

References

Tables

Figures

◀

▶

◀

▶

Back

Close

Full Screen / Esc

Printer-friendly Version

Interactive Discussion



observed here may be the result of iodine emission from macroalgae beds located further away. Indeed, back-trajectory calculations of the path of the air mass arriving at the site show that the air spent significant time travelling along the coast to the north-west of the site, where large macroalgae beds are located.

Models of fast photochemistry at Mace Head have highlighted the impact of halogens on HO_x. Sommariva et al. (2006) used an in situ box model to show that observed HO₂ could be reproduced by increasing the maximum spatially-averaged IO concentrations observed by an order of magnitude. In the presence of 50 ppt IO, the modelled HO₂ concentration was reduced by 50% and the modelled OH increased by 30%, in close agreement with observed values. The formation (Reaction R12) and photolysis of HOI (Reaction R13):



was found to be the dominant HO₂ → OH pathway, more than an order of magnitude greater than the normally dominant HO₂ + NO → OH + NO₂ pathway.

The point observations of IO presented here show that mixing ratios of IO greater than 10 pptv are only present at tide heights below 1 m. This suggests that iodine related chemistry dominates the HO_x budget at Mace Head during the low tide periods of spring tides.

5 Conclusions

Point measurements of IO were made at Mace Head Atmospheric Research Station, a clean marine site on the west coast of Ireland. IO was found to be highly variable, with up to 49.8 pptv IO observed (1 s). IO showed a strong anti-correlation with daytime low tide and the associated local macroalgae exposure. IO peaked in the hour after low tide, an offset which may be due to the time required for desiccation and oxidative

Temporal variability and spatial distribution of IO

R. Commane et al.

Title Page

Abstract

Introduction

Conclusions

References

Tables

Figures

⏪

⏩

◀

▶

Back

Close

Full Screen / Esc

Printer-friendly Version

Interactive Discussion



stressing of macroalgae, as well as mechanical agitation from returning waves. This is consistent with previous aerosol observations, which saw a peak in < 10 nm particle number in the hour after low tide. No IO mixing ratios above the instrumental limit of detection were observed at night.

5 A comparison of spatially-averaged long-path Differential Optical Absorption Spectroscopy (LP-DOAS) observations of IO with point observations of IO by LIF showed similar temporal trends. However LP-DOAS reported a factor of between 6 and 10 times less than the LIF observations of IO, consistent with the assumption of inhomogeneities of IO along the LP-DOAS light-path used to explain previous radical point
10 measurements.

Overall the observations presented here found that coastal areas influenced by macroalgae contain high concentrations of IO but only for short periods of time (day-time low tide). While these high concentrations of IO may significantly perturb local oxidation chemistry, this large effect will be relatively short-lived.

15 *Acknowledgements.* The authors would like to thank the staff at the Mace Head Atmospheric Research Station and NUI Galway, in particular Prof. G. Jennings and Dr. G. Spain. Meteorological and supporting measurements were provided by G. Spain (University of Bristol) and B. Kelly (NUIG/Met Éireann). Support for access to Mace Head was given by the European Community – Research Infrastructure Action under EUSAAR TNA programme. The LP-DOAS
20 deployment was conducted under the MAP Project funded by the European Commission (under FP6 project number 018332). Tidal data reproduced by permission of the Controller of Her Majesty's Stationery Office and the UK Hydrographic Office (www.ukho.gov.uk). We are grateful for the expert technical support from the workshops in the School of Chemistry at the University of Leeds.

Temporal variability and spatial distribution of IO

R. Commane et al.

[Title Page](#)[Abstract](#)[Introduction](#)[Conclusions](#)[References](#)[Tables](#)[Figures](#)[⏪](#)[⏩](#)[◀](#)[▶](#)[Back](#)[Close](#)[Full Screen / Esc](#)[Printer-friendly Version](#)[Interactive Discussion](#)

References

- Alicke, B., Hebestreit, K., Stutz, J., and Platt, U.: Iodine oxide in the marine boundary layer, *Nature*, 397, 572–573, 1999. 4534, 4535, 4536
- Axelson, H., Galle, B., Gustavson, K., Ragnarsson, P., and Rudin, M.: A transmitting/receiving telescope for DOAS-measurements using retroreflektor technique, *Techn. Dig. S.*, 4, 641–644, 1990. 4548
- Bale, C. S. E., Ingham, T., Commane, R., Heard, D. E., and Bloss, W. J.: Novel measurements of atmospheric iodine species by resonance fluorescence, *J. Atmos. Chem.*, 60, 51–70, doi:10.1007/s10874-008-9108-z, <http://www.springerlink.com/content/k6j323266406772j>, 2008. 4535, 4546
- Ball, S. M., Hollingsworth, A. M., Humbles, J., Leblanc, C., Potin, P., and McFiggans, G.: Spectroscopic studies of molecular iodine emitted into the gas phase by seaweed, *Atmos. Chem. Phys.*, 10, 6237–6254, doi:10.5194/acp-10-6237-2010, 2010. 4535, 4546
- Bitter, M., Ball, S. M., Povey, I. M., and Jones, R. L.: A broadband cavity ringdown spectrometer for in-situ measurements of atmospheric trace gases, *Atmos. Chem. Phys.*, 5, 2547–2560, doi:10.5194/acp-5-2547-2005, 2005. 4547
- Bloss, W. J., Lee, J. D., Johnson, G. P., Sommariva, R., Heard, D. E., Saiz-Lopez, A., Plane, J. M. C., McFiggans, G., Coe, H., Flynn, M., Williams, P., Rickard, A. R., and Fleming, Z. L.: Impact of halogen monoxide chemistry upon boundary layer OH and HO₂ concentrations at a coastal site, *Geophys. Res. Lett.*, 32, L06814, doi:10.1029/2004GL022084, 2005. 4534
- Burkholder, J. B., Curtius, J., Ravishankara, A. R., and Lovejoy, E. R.: Laboratory studies of the homogeneous nucleation of iodine oxides, *Atmos. Chem. Phys.*, 4, 19–34, doi:10.5194/acp-4-19-2004, 2004. 4535, 4544
- Carpenter, L. J., Hebestreit, K., Platt, U., and Liss, P. S.: Coastal zone production of IO precursors: a 2-dimensional study, *Atmos. Chem. Phys.*, 1, 9–18, doi:10.5194/acp-1-9-2001, 2001. 4535, 4550, 4567
- Chambers, R. M., Heard, A. C., and Wayne, R. P.: Inorganic gas-phase reactions of the nitrate radical: iodine + nitrate radical and iodine atom + nitrate radical, *J. Phys. Chem.*, 96, 3321–3331, doi:10.1021/j100187a028, 1992. 4547
- Commane, R., Floquet, C. F. A., Ingham, T., Stone, D., Evans, M. J., and Heard, D. E.: Observations of OH and HO₂ radicals over West Africa, *Atmos. Chem. Phys.*, 10, 8783–8801,

Temporal variability and spatial distribution of IO

R. Commane et al.

Title Page

Abstract

Introduction

Conclusions

References

Tables

Figures

◀

▶

◀

▶

Back

Close

Full Screen / Esc

Printer-friendly Version

Interactive Discussion



Temporal variability and spatial distribution of IO

R. Commane et al.

Title Page

Abstract

Introduction

Conclusions

References

Tables

Figures

◀

▶

◀

▶

Back

Close

Full Screen / Esc

Printer-friendly Version

Interactive Discussion



doi:10.5194/acp-10-8783-2010, 2010.

Davis, D., Crawford, J., Liu, S., McKeen, S., Bandy, A., Rowland, D. T. F., and Blake, D.: Potential impact of iodine on tropospheric levels of ozone; other critical oxidants, *J. Geophys. Res.-Atmos.*, 101, 2135–2147, 1996. 4538, 4541

4534

Dixneuf, S., Ruth, A. A., Vaughan, S., Varma, R. M., and Orphal, J.: The time dependence of molecular iodine emission from *Laminaria digitata*, *Atmos. Chem. Phys.*, 9, 823–829, doi:10.5194/acp-9-823-2009, 2009. 4535, 4546

Furneaux, K. L., Whalley, L. K., Heard, D. E., Atkinson, H. M., Bloss, W. J., Flynn, M. J., Gallagher, M. W., Ingham, T., Kramer, L., Lee, J. D., Leigh, R., McFiggans, G. B., Mahajan, A. S., Monks, P. S., Oetjen, H., Plane, J. M. C., and Whitehead, J. D.: Measurements of iodine monoxide at a semi polluted coastal location, *Atmos. Chem. Phys.*, 10, 3645–3663, doi:10.5194/acp-10-3645-2010, 2010. 4537, 4544, 4546, 4550, 4551, 4567

Gilles, M. K., Turnipseed, A. A., Talukdar, R. K., Rudich, Y., Villalta, P. W., Huey, L. G., Burkholder, J. B., and Ravishankara, A. R.: Reactions of O(³P) with alkyl iodides: rate coefficients and reaction products, *J. Phys. Chem.*, 100, 14005–14015, 1996. 4541

Gravestock, T. J., Blitz, M. A., and Heard, D. E.: A laser induced fluorescence study relating to physical properties of the iodine monoxide radical, *Phys. Chem. Chem. Phys.*, 4, 823–834, 2010. 4537, 4538

Heard, D. E., Read, K. A., Methven, J., Al-Haider, S., Bloss, W. J., Johnson, G. P., Pilling, M. J., Seakins, P. W., Smith, S. C., Sommariva, R., Stanton, J. C., Still, T. J., Ingham, T., Brooks, B., De Leeuw, G., Jackson, A. V., McQuaid, J. B., Morgan, R., Smith, M. H., Carpenter, L. J., Carslaw, N., Hamilton, J., Hopkins, J. R., Lee, J. D., Lewis, A. C., Purvis, R. M., Wevill, D. J., Brough, N., Green, T., Mills, G., Penkett, S. A., Plane, J. M. C., Saiz-Lopez, A., Worton, D., Monks, P. S., Fleming, Z., Rickard, A. R., Alfarra, M. R., Allan, J. D., Bower, K., Coe, H., Cubison, M., Flynn, M., McFiggans, G., Gallagher, M., Norton, E. G., O'Dowd, C. D., Shillito, J., Topping, D., Vaughan, G., Williams, P., Bitter, M., Ball, S. M., Jones, R. L., Povey, I. M., O'Doherty, S., Simmonds, P. G., Allen, A., Kinnersley, R. P., Beddows, D. C. S., Dall'Osto, M., Harrison, R. M., Donovan, R. J., Heal, M. R., Jennings, S. G., Noone, C., and Spain, G.: The North Atlantic Marine Boundary Layer Experiment(NAMBLEX). Overview of the campaign held at Mace Head, Ireland, in summer 2002, *Atmos. Chem. Phys.*, 6, 2241–2272, doi:10.5194/acp-6-2241-2006, 2006. 4536

Huang, R.-J., Seitz, K., Buxmann, J., Pöhler, D., Hornsby, K. E., Carpenter, L. J., Platt, U., and

**Temporal variability
and spatial
distribution of IO**

R. Commane et al.

Title Page

Abstract

Introduction

Conclusions

References

Tables

Figures

◀

▶

◀

▶

Back

Close

Full Screen / Esc

Printer-friendly Version

Interactive Discussion



Hoffmann, T.: In situ measurements of molecular iodine in the marine boundary layer: the link to macroalgae and the implications for O_3 , IO, OIO and NO_x , *Atmos. Chem. Phys.*, 10, 4823–4833, doi:10.5194/acp-10-4823-2010, 2010. 4548

5 Kaltsoyannis, N. and Plane, J. M. C.: Quantum chemical calculations on a selection of iodine-containing species (IO, OIO, INO_3 , $(IO)_2$, I_2O_3 , I_2O_4 and I_2O_5) of importance in the atmosphere, *Phys. Chem. Chem. Phys.*, 10, 1723–1733, doi:10.1039/b715687c, 2008. 4535, 4544

Kraus, S.: DOASIS: a framework design for DOAS, Ph.D. thesis, Combined Faculties for Mathematics and for Computer Science, University of Mannheim, 2005. 4548

10 Küpper, F. C., Carpenter, L. J., McFiggans, G. B., Palmer, C. J., Waite, T. J., Boneberg, E.-M., Woitsch, S., Weiller, M., Abela, R., Grolimund, D., Potin, P., Butler, A., Luther, G. W., Kroeck, P. M. H., Meyer-Klaucke, W., and Feiters, M. C.: Iodide accumulation provides help with an inorganic antioxidant impacting atmospheric chemistry, *P. Natl. Acad. Sci. USA*, 105, 6954–6958, doi:10.1073/pnas.0709959105, http://www.pnas.org/content/105/19/6954.abstract, 2008. 4546

15 Mäkelä, J. M., Hoffmann, T., Holzke, C., Väkevä, M., Suni, T., Mattila, T., Aalto, P. P., Tapper, U., Kauppinen, E. I., and O'Dowd, C. D.: Biogenic iodine emissions and identification of end-products in coastal ultrafine particles during nucleation bursts, *J. Geophys. Res.*, 107, 8110, doi:10.1029/2001JD000580, 2002. 4534

20 Merten, A., Tschritter, J., and Platt, U.: Novel design of DOAS-long-path telescopes based on fiber optics, *Appl. Optics*, in press, 2009. 4548

McFiggans, G., Coe, H., Burgess, R., Allan, J., Cubison, M., Alfarra, M. R., Saunders, R., Saiz-Lopez, A., Plane, J. M. C., Wevill, D., Carpenter, L., Rickard, A. R., and Monks, P. S.: Direct evidence for coastal iodine particles from *Laminaria* macroalgae – linkage to emissions of molecular iodine, *Atmos. Chem. Phys.*, 4, 701–713, doi:10.5194/acp-4-701-2004, 2004. 4535, 4546, 4551

O'Dowd, C. D. and Hoffmann, T.: Coastal new particle formation: a review of the current state-of-the-art, *Environ. Chem.*, 2, 245, doi:10.1071/EN05077, 2005. 4545

25 O'Dowd, C. D., Jimenez, J. L., Bahreini, R., Flagan, R. C., Seinfeld, J. H., Hameri, K., Pirjola, L., Kulmala, M., and Jennings, S. G.: Marine aerosol formation from biogenic emissions, *Nature*, 417, 632–636, 2002. 4534, 4535

30 Platt, U. and Stutz, J.: *Differential Optical Absorption Spectroscopy, Principles and Applications*, Physics of Earth and Space Environments Volume, Springer-Verlag Berlin Heidelberg,

ISBN:978-3-540-21193-8, 2008. 4548

Rosenfeld, D., Lohmann, U., Raga, G., O'Dowd, C., Kulmala, M., Fuzzi, S., Reissell, A., and Andreae, M.: Flood or drought: how do aerosols affect precipitation?, *Science*, 321, 1309–1313, 2008. 4535

5 Rothman, L. S., Jacquemart, D., Barbe, A., Benner, D., Birk, M., Brown, L. R., Carleer, M. R. C. C. J., Chance, K., Coudert, L. H., Dana, V., Devi, V. M., Flaud, J.-M., Gamache, R. R., Goldman, R., Hartmann, J.-M., Jucks, K. W., Maki, A. G., Mandin, J.-Y., Massie, S. T., Orphal, J., Perrin, A., Rinsland, C. P., Smith, M. A. H., Tennyson, J., Tolchenov, R. N., Toth, R., Auwera, J. V., Varanasi, P., and Wagner, G.: The HITRAN 2004 molecular spectroscopic database, *J. Quant. Spectrosc. Ra.*, 96, 139–204, 2005. 4548

10 Saiz-Lopez, A., Shillito, J. A., Coe, H., and Plane, J. M. C.: Measurements and modelling of I₂, IO, OIO, BrO and NO₃ in the mid-latitude marine boundary layer, *Atmos. Chem. Phys.*, 6, 1513–1528, doi:10.5194/acp-6-1513-2006, 2006a. 4535, 4536

15 Saiz-Lopez, A., Plane, J. M. C., McFiggans, G., Williams, P. I., Ball, S. M., Bitter, M., Jones, R. L., Hongwei, C., and Hoffmann, T.: Modelling molecular iodine emissions in a coastal marine environment: the link to new particle formation, *Atmos. Chem. Phys.*, 6, 883–895, doi:10.5194/acp-6-883-2006, 2006b. 4547, 4550

20 Sander, S. P., Friedl, R. R., Golden, D. M., Kurylo, M. J., Moortgat, C. K., Keller-Rudek, H., Wine, P. H., Ravishankara, A. R., Kolb, C. E., Molina, M. J., Finlayson-Pitts, B. J., Orkin, V. L., and Huie, R. E.: Chemical kinetics and photochemical data for use in stratospheric studies, Evaluation number 15, NASA Jet Propulsion Laboratory, Publication 06-2, 2006. 4541, 4547

25 Seitz, K., Buxmann, J., Pöhler, D., Sommer, T., Tschirter, J., Neary, T., O'Dowd, C., and Platt, U.: The spatial distribution of the reactive iodine species IO from simultaneous active and passive DOAS observations, *Atmos. Chem. Phys.*, 10, 2117–2128, doi:10.5194/acp-10-2117-2010, 2010. 4536, 4545, 4549

Sellegrì, K., Yoon, Y. J., Jennings, S. G., O'Dowd, C. D., Pirjola, L., Cautenet, S., Chen, H., and Hoffmann, T.: Quantification of Coastal New Ultra-Fine Particles Formation from In situ and Chamber Measurements during the BIOFLUX Campaign, *Environ. Chem.*, 2(4), 260-270, doi:10.1071/EN05074, 2005. 4534

30 Sommariva, R., Bloss, W. J., Brough, N., Carslaw, N., Flynn, M., Haggerstone, A.-L., Heard, D. E., Hopkins, J. R., Lee, J. D., Lewis, A. C., McFiggans, G., Monks, P. S., Penkett, S. A., Pilling, M. J., Plane, J. M. C., Read, K. A., Saiz-Lopez, A., Rickard, A. R., and Williams, P. I.: OH and HO₂ chemistry during NAMBLEX: roles of oxygenates, halogen ox-

Temporal variability and spatial distribution of IO

R. Commane et al.

Title Page

Abstract

Introduction

Conclusions

References

Tables

Figures

◀

▶

◀

▶

Back

Close

Full Screen / Esc

Printer-friendly Version

Interactive Discussion



ides and heterogeneous uptake, *Atmos. Chem. Phys.*, 6, 1135–1153, doi:10.5194/acp-6-1135-2006, 2006. 4536, 4552

Spietz, P., Gomez-Martin, J., and Burrows, J. P.: Spectroscopic studies of the I_2/O_3 photochemistry. Part 2. Improved spectra of iodine oxides and analysis of the IO absorption spectrum, *J. Photoch. Photobio. A*, 176, 50–67, 2005. 4548

Stutz, J. and Platt, U.: Numerical analysis and estimation of the statistical error of differential optical absorption spectroscopy measurements with least-squares methods, *Appl. Optics*, 35, 6041–6053, 1996. 4548

Voigt, S., Orphal, J., and Burrows, J. P.: The temperature and pressure dependence of the absorption cross-sections of NO_2 in the 250–800 nm region measured by Fourier-transform spectroscopy, *J. Photoch. Photobio. A*, 149, 1–7, 2002. 4548

Wada, R., Beames, J. M., and Orr-Ewing, A. J.: Measurement of IO radical concentrations in the marine boundary layer using a cavity ring-down spectrometer, *J. Atmos. Chem.*, 58, 69–87, 2007. 4550

Whitehead, J. D., McFiggans, G. B., Gallagher, M. W., and Flynn, M. J.: Direct linkage between tidally driven coastal ozone deposition fluxes, particle emission fluxes, and subsequent CCN formation, *J. Geophys. Res.*, 36, L04806, doi:10.1029/2008GL035969, 2009. 4551

Whalley, L. K., Furneaux, K. L., Gravestock, T., Atkinson, H. M., Bale, C. S. E., Ingham, T., Bloss, W. J., and Heard, D. E.: Detection of iodine monoxide radicals in the marine boundary layer using laser induced fluorescence spectroscopy, *J. Atmos. Chem.*, 58, 19–39, 2007. 4537, 4542

Yokelson, R. J., Burkholder, J. B., Fox, R. W., Talukdar, R. K., and Ravishankara, A. R.: Temperature dependence of the NO_3 absorption spectrum, *J. Phys. Chem.*, 98, 13144–13150, 1994. 4548

**Temporal variability
and spatial
distribution of IO**R. Commane et al.

[Title Page](#)[Abstract](#)[Introduction](#)[Conclusions](#)[References](#)[Tables](#)[Figures](#)[◀](#)[▶](#)[◀](#)[▶](#)[Back](#)[Close](#)[Full Screen / Esc](#)[Printer-friendly Version](#)[Interactive Discussion](#)

Temporal variability and spatial distribution of IO

R. Commane et al.

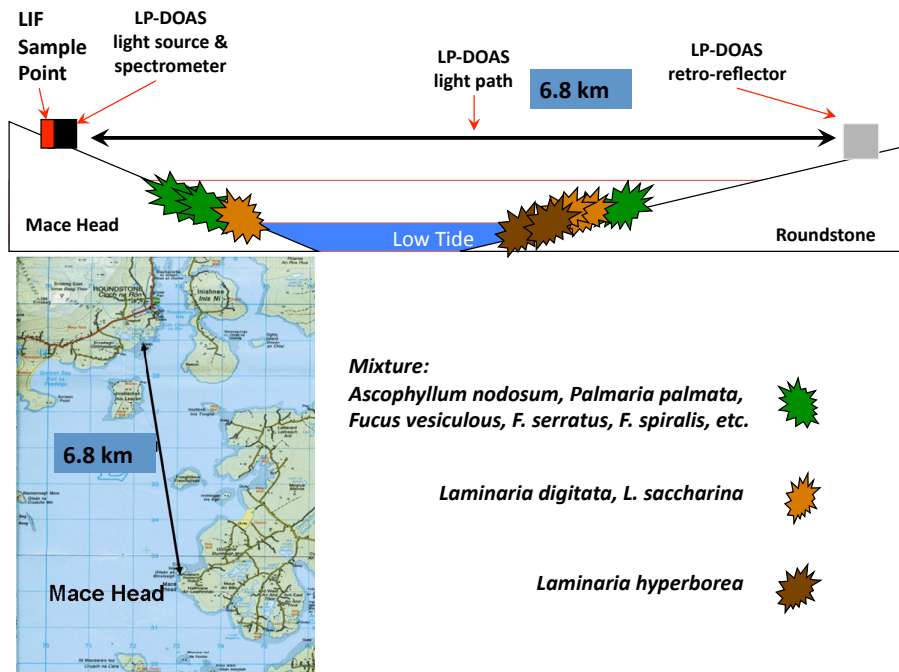


Fig. 1. (Top): Schematic representation of the position of the in situ LIF sampling point and LP-DOAS light path. Extensive *Laminaria* beds were observed in the inter-tidal areas under the LP-DOAS light path. (Bottom): Map of Mace Head showing the 6.8 km LP-DOAS light path between Mace Head and Roundstone.

Title Page

Abstract

Introduction

Conclusions

References

Tables

Figures

◀

▶

◀

▶

Back

Close

Full Screen / Esc

Printer-friendly Version

Interactive Discussion



**Temporal variability
and spatial
distribution of IO**

R. Commane et al.

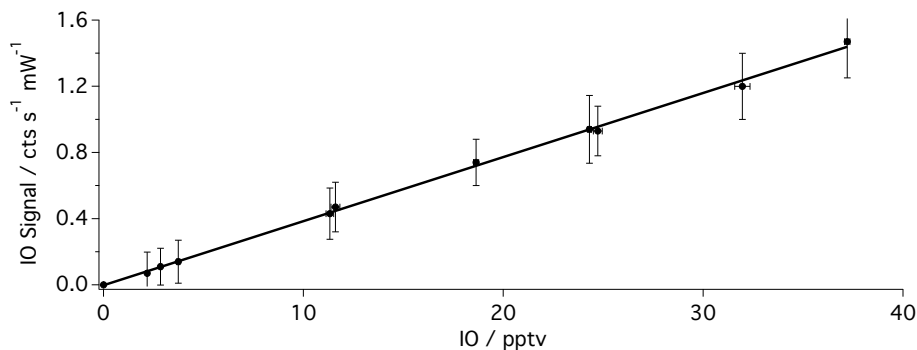


Fig. 2. Calibration of IO for mixing ratios between 2.2 and 37.2 pptv. From this fit, the sensitivity of the instrument (C_{IO}) is $0.039 (\pm 0.001) \text{ cts s}^{-1} \text{ mW}^{-1} \text{ pptv}^{-1}$, with a slight negative intercept ($-0.002 (\pm 0.01) \text{ cts s}^{-1} \text{ mW}^{-1}$), $R = 0.999$.

Title Page

Abstract

Introduction

Conclusions

References

Tables

Figures

◀

▶

◀

▶

Back

Close

Full Screen / Esc

Printer-friendly Version

Interactive Discussion



Temporal variability and spatial distribution of IO

R. Commane et al.

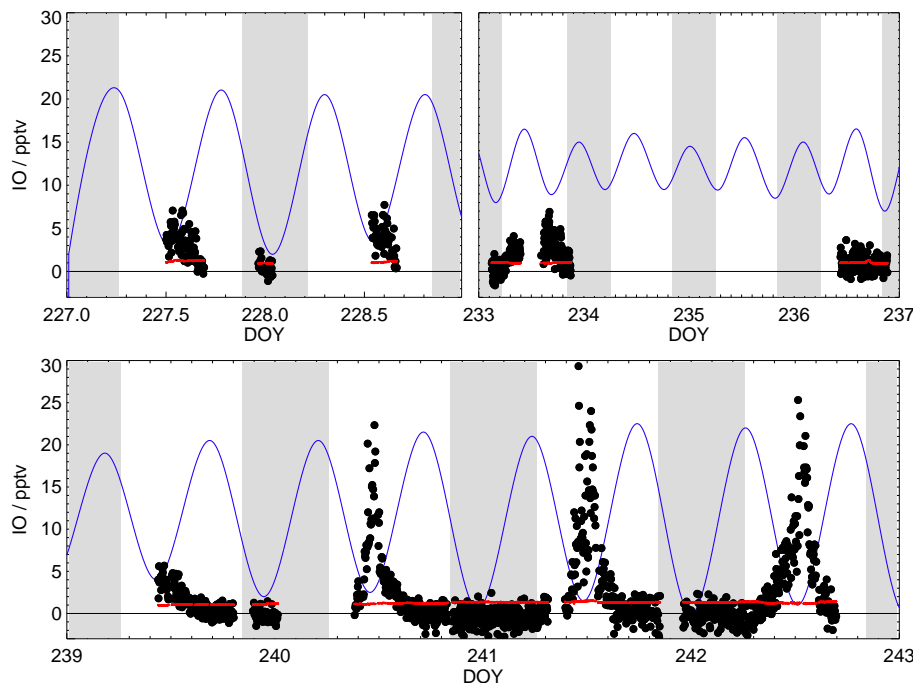


Fig. 3. IO mixing ratio (pptv) observed by LIF for a 60 s time integration period (black) for the Day of Year (DOY) in 2007; IO instrument 60 s limit of detection (~ 1.4 pptv at 2σ) (red); predicted tide height at Roundstone Bay (blue) scaled to fit the graph. Shaded areas indicate night-time observations. Data were collected between 15 (DOY 227) and 30 August (DOY 242) 2007.

[Title Page](#)
[Abstract](#)
[Introduction](#)
[Conclusions](#)
[References](#)
[Tables](#)
[Figures](#)
[◀](#)
[▶](#)
[◀](#)
[▶](#)
[Back](#)
[Close](#)
[Full Screen / Esc](#)
[Printer-friendly Version](#)
[Interactive Discussion](#)


Temporal variability and spatial distribution of IO

R. Commane et al.

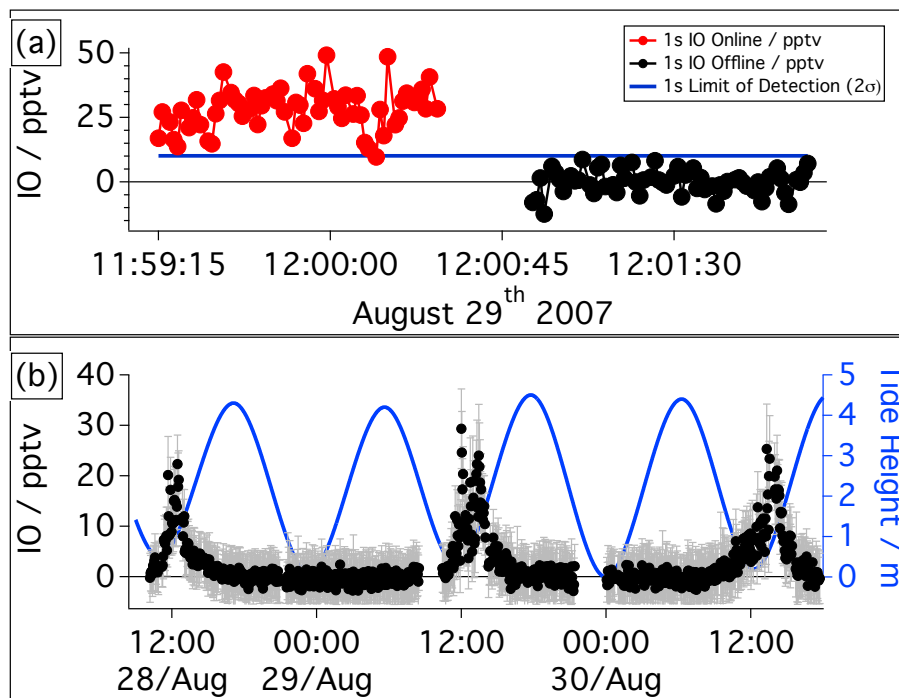


Fig. 4. (a) 1 s IO mixing ratio (pptv) (red) at noon on 29 August (DOY 241) in 2007. The 1 s background signal converted to an equivalent IO mixing ratio is indicated as “offline” and shown in black. The 1 s limit of detection (2σ) shown in blue. Up to $49.7(\pm 8.6)$ pptv IO was observed over this short time scale. (b) 60 s IO mixing ratio (pptv; black) with the standard deviation of the 1 s data within the 60 s block average shown as error bars (grey). Tide height is shown as a blue line.

Title Page

Abstract

Introduction

Conclusions

References

Tables

Figures

◀

▶

◀

▶

Back

Close

Full Screen / Esc

Printer-friendly Version

Interactive Discussion



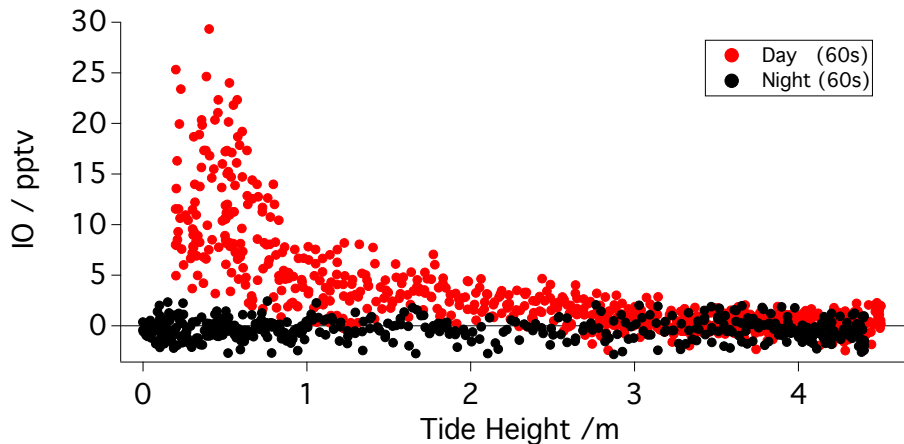


Fig. 5. IO mixing ratio observed by LIF (60 s integration time) against tide height: day (red), night (black). A clear anti-correlation of IO with tide height can be seen during daylight hours but there is no tidal dependence at night.

Temporal variability and spatial distribution of IO

R. Commane et al.

Title Page

Abstract

Introduction

Conclusions

References

Tables

Figures

◀

▶

◀

▶

Back

Close

Full Screen / Esc

Printer-friendly Version

Interactive Discussion



**Temporal variability
and spatial
distribution of IO**

R. Commane et al.

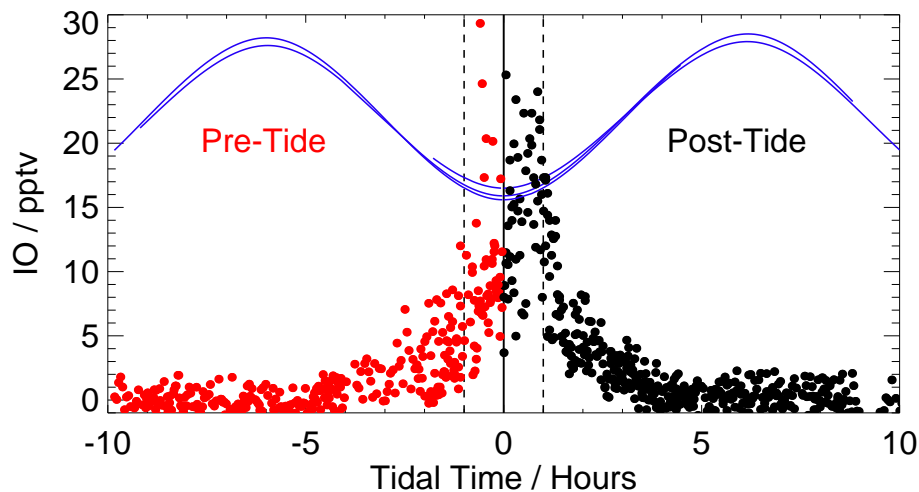


Fig. 6. IO mixing ratio as a function of time from daytime low tide for all data between 28–30 August. Data are separated between before (red) and after (black) daytime low tide. The hour before and after low tide is indicated by black dashed lines.

[Title Page](#)[Abstract](#)[Introduction](#)[Conclusions](#)[References](#)[Tables](#)[Figures](#)[◀](#)[▶](#)[◀](#)[▶](#)[Back](#)[Close](#)[Full Screen / Esc](#)[Printer-friendly Version](#)[Interactive Discussion](#)

**Temporal variability
and spatial
distribution of IO**

R. Commane et al.

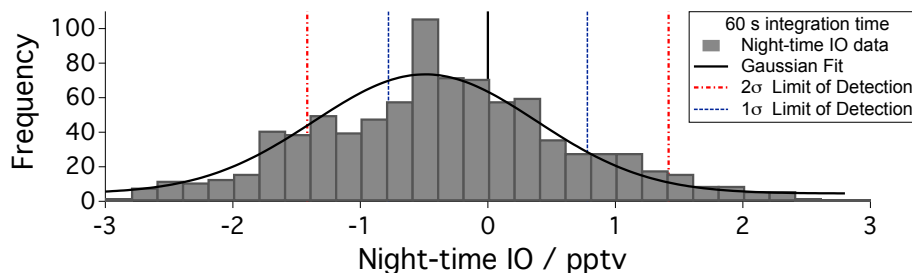


Fig. 7. Histogram of night-time IO data (60 s integration time; grey boxes), \pm LOD ($2\sigma = 1.4$ pptv; red dash-dot lines, $1\sigma = 0.78$ pptv; blue dashed lines). A Gaussian fit to these data (black line) shows a slight negative bias (-0.49 pptv).

[Title Page](#)[Abstract](#)[Introduction](#)[Conclusions](#)[References](#)[Tables](#)[Figures](#)[◀](#)[▶](#)[◀](#)[▶](#)[Back](#)[Close](#)[Full Screen / Esc](#)[Printer-friendly Version](#)[Interactive Discussion](#)

Temporal variability and spatial distribution of IO

R. Commane et al.

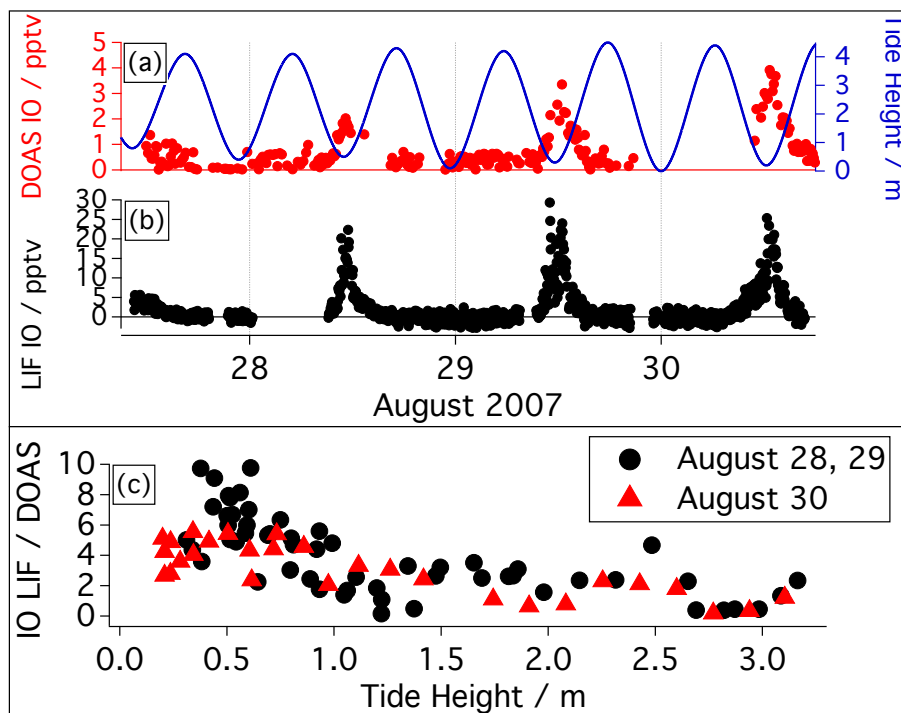


Fig. 8. Observation of LP-DOAS and LIF IO between 28–30 August. **(a)** LP-DOAS IO (pptv, red, 10 min), tide height (blue), **(b)** LIF IO (pptv, black, 1 min), **(c)** anti-correlation of the LIF/LP-DOAS IO ratio with tide height down to 0.3 m. 30 August (red triangles) shows a lower ratio than 28–29 August (black dots). This corresponds to increased IO detected by the LP-DOAS on 30 August.

Title Page

Abstract

Introduction

Conclusions

References

Tables

Figures

◀

▶

◀

▶

Back

Close

Full Screen / Esc

Printer-friendly Version

Interactive Discussion



Temporal variability and spatial distribution of IO

R. Commane et al.

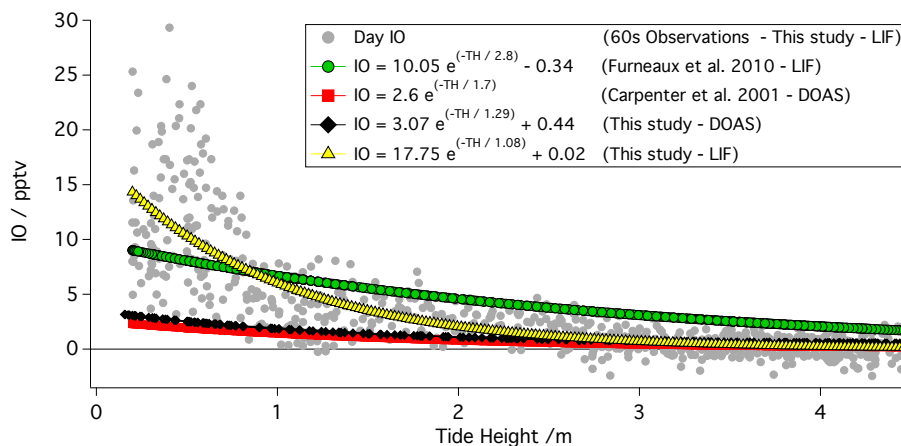


Fig. 9. IO as a function of tide compared to other studies. Point observations of IO by LIF presented in this study (one minute data: grey points, tidal dependence: yellow triangles), Furneaux et al. (2010) point observations by LIF at Roscoff, France (green points), Carpenter et al. (2001) LP-DOAS observations at Mace Head (red squares), LP-DOAS observations from this study (black diamonds). Point observations of IO (by LIF) show the strongest dependence on tide height.

Title Page

Abstract

Introduction

Conclusions

References

Tables

Figures

◀

▶

◀

▶

Back

Close

Full Screen / Esc

Printer-friendly Version

Interactive Discussion



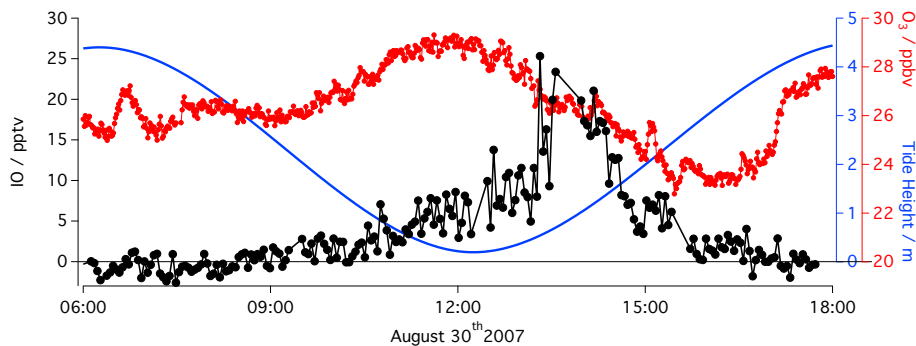


Fig. 10. Time series of IO and O₃ (60 s) and tidal height (m) for 30 August, 2007.

Temporal variability and spatial distribution of IO

R. Commane et al.

Title Page

Abstract

Introduction

Conclusions

References

Tables

Figures

◀

▶

◀

▶

Back

Close

Full Screen / Esc

Printer-friendly Version

Interactive Discussion

